

PACS numbers: 42.70.Hj; 42.55.Rz; 42.25.Gy
DOI: 10.1070/QE2006v036n05ABEH013230

Mechanisms of a change in the refractive index of an intensely pumped Yb : YAG crystal

O.L. Antipov, D.V. Bredikhin, O.N. Eremeykin, E.V. Ivakin,
A.P. Savikin, A.V. Sukhodolov, K.A. Fedorova

***Abstract*. Mechanisms of a change in the refractive index appearing in an intensely diode-pumped Yb : YAG-laser disk element are studied with the help of polarisation interferometry and dynamic grating testing. It is found that changes in the electronic component of the refractive index arising upon changing the populations of electronic levels of Yb^{3+} ions (the ground $^2F_{7/2}$ state and the upper $^2F_{5/2}$ level of the laser transition) and caused by the difference in the polarisability of these levels are an order of magnitude greater than thermal changes in the refractive index. It is shown that the difference Δp in the polarisability at the probe wavelength of 633 nm is 1.9×10^{-26} cm^3 and at the laser transition wavelength of 1029 nm is 1.6×10^{-26} cm^3.**

Keywords: *laser crystals and glasses, Yb : YAG crystal, changes in the refractive index, polarisability, nonlinear optical properties.*

1. Introduction

Intense pumping of laser crystals is accompanied by considerable changes in their refractive index, which limit the lasing power and the quality of the light beam in laser amplifiers and generators. The refractive index changes (RICs) in laser crystals upon pumping are caused both by thermal heating and changes in the excited-level populations of activator ions (Nd^{3+}, Yb^{3+}, Tm^{3+}, etc.). The RIC caused by a change in the electronic level populations is explained by the difference in the polarisability of these levels [1 – 4]. It has been shown earlier that upon intensive diode pumping of Nd^{3+}-doped laser crystals and glasses, the electronic component of RICs can be comparable with the thermal component [2 – 4].

Laser crystals and glasses doped with Yb^{3+} ions are of current interest as the most promising materials for active media of high-power solid-state diode-pumped lasers [5 – 7]. The energy level diagram of Yb^{3+} ions in such laser materials provides a small difference between the pump and lasing photons as well as absence of up-conversion effects and excited-state absorption (Fig. 1). Due to this, thermal distortions of beams in such laser media are minimal and electronic RICs caused by the difference between polarisabilities of excited and nonexcited Yb^{3+} ions can become dominating. Recent studies have shown that strong electronic RICs in ytterbium-doped fibre lasers can play a significant role in processes of summation of radiation from multichannel lasers [8]. However, information on electronic RICs in Yb-doped laser crystals has not been available so far.

This paper is devoted to the study of RIC mechanisms in an intensely diode-pumped Yb : YAG crystal with the help of polarisation interferometry and dynamic grating methods. The aim of this paper is to determine the contributions of electronic and thermal RIC components.

2. Interferometric measurements

Changes in the refractive index in a diode-pumped Yb : YAG crystal were studied with a compact highly sensitive Jamin – Lebedev polarisation interferometer

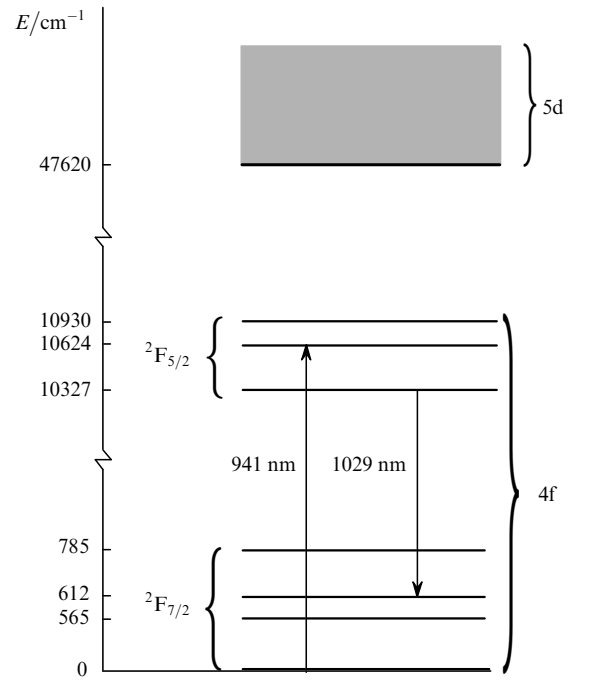

Figure 1. Energy level diagram of Yb^{3+} ions in a Yb : YAG crystal.

O.L. Antipov, D.V. Bredikhin, O.N. Eremeykin, A.P. Savikin, K.A. Fedorova Institute of Applied Physics, Russian Academy of Sciences, ul. Ul'yanova 46, 603600 Nizhnii Novgorod, Russia; e-mail: antipov@appl.sci-nnov.ru;
E.V. Ivakin, A.V. Sukhodolov B.I. Stepanov Institute of Physics, National Academy of Sciences of Belarus, prosp. Nezavisimosti 70, 220072 Minsk, Belarus; e-mail: ivakin@dragon.bas-net.by

Received 2 March 2006
Kvantovaya Elektronika **36** (5) 418 – 423 (2006)
Translated by I.A. Ulitkin

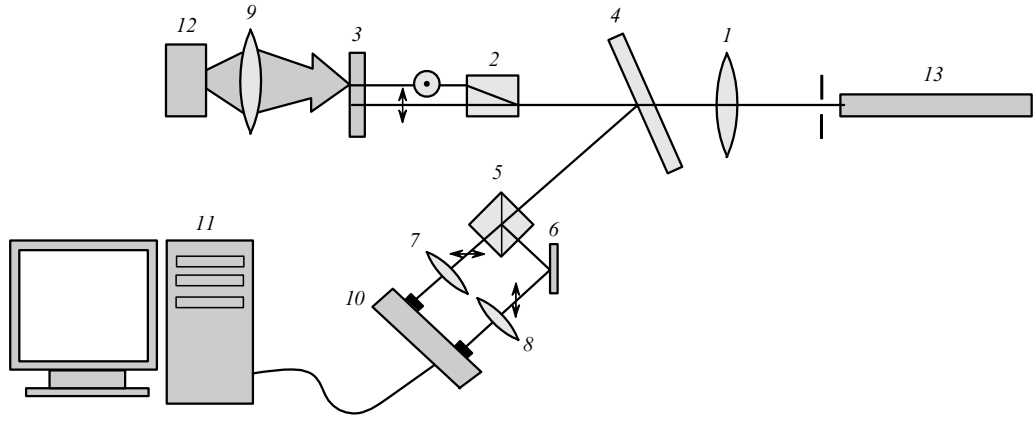

Figure 2. Scheme of the polarisation interferometer: (*1*, *7–9*) lenses; (*2*) polarisation beamsplitter; (*3*) Yb : YAG disk with a mirror for 633 nm; (*4*) semitransparent mirror; (*5*) Glan's prism; (*6*) mirror; (*10*) two-channel detector with an electronic differential amplifier; (*11*) signal analyser; (*12*) diode laser ($\lambda = 633$ nm); (*13*) He–Ne laser.

(Fig. 2). Measurements were performed in a 400-μm thick Yb : YAG-crystal disk (ELS-94 Ltd, Moscow) of diameter 6 mm. The crystal was doped with Yb^{3+} ions with the atomic concentration of ~9 %. A broadband InGaAsP/GaAs heterostructure laser diode (fabricated at the Physics and Technology Institute at the Nizhnii Novgorod State University) emitting ~1-ms, 6-W pulses at 941 nm was used for pumping. The pump beam was focused by a system of lenses into a region of size $\sim 0.15 \times 1.0$ mm on the Yb : YAG disk. Two probe orthogonally polarised beams from a 633-nm, 15-mW He–Ne laser propagated in the disk through the pumped and non-pumped regions (the distance between probe beams was ~1.5 mm, their diameters in the sample being ~100 μm). The results of measurements of the phase shift caused by pumping were averaged over more than 500 pulses, which reduced the phase measurement errors in the interferometer down to $\sim 10^{-3}$.

The RIC dynamics was measured during the pump pulse and after its termination. A quasi-linear increase and a decrease in the RICs were observed respectively in oscillograms during this pulse and after its termination (Fig. 3). The maximum RIC at the end of the pump pulse was $\sim 7 \times 10^{-6}$. The detected signal was described with a high accuracy by the sum of two exponentials: $Y = Y_0 + A_1 \exp(-t/t_1) + A_2 \exp(-t/t_2)$. A stronger fast component had the characteristic time $t_1 \approx 0.9 - 1.0$ ms, which was independent of the focal length of lens (*9*) (Fig. 2). This relaxation time corresponds to the lifetime of the metastable $^2F_{7/2}$ level of a working laser transition T_e in a Yb : YAG crystal. Therefore, this component can be identified with electronic RICs Δn_e, caused by the difference Δp in polarisabilities of the ground $^2F_{7/2}$ state and excited metastable $^2F_{5/2}$ level, which can be described by the expression [1, 2]:

$$\Delta n_e = \frac{2\pi F_L^2}{n_0} \Delta p \Delta N, \tag{1}$$

where $F_L^2 = (n_0^2 + 2)/3$ is the local field factor (Lorentz factor); n_0 is the unperturbed refractive index; ΔN is the change in the populations of the $^2F_{5/2}$ and $^2F_{7/2}$ levels. The second slowly varying component [with the characteristic time t_2 increasing from 3 to 7 ms with increasing the focal length of lens (*9*)] can be defined as a thermal RIC and described by the expression:

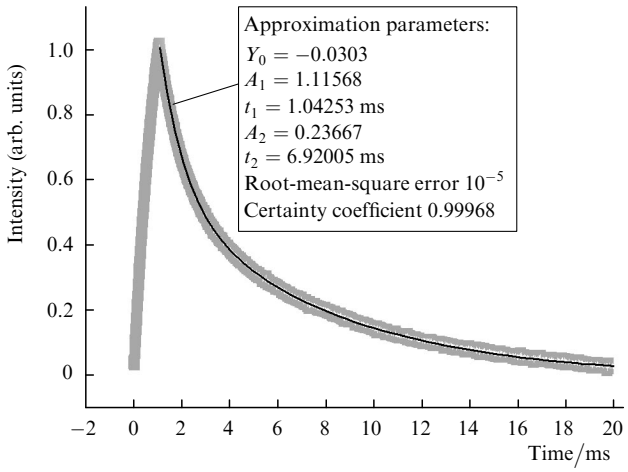

Figure 3. Typical experimental oscillogram of RICs (wide grey curve) and its approximation by the sum of two exponentials (solid curve) for a ~2-W pump power. The approximation parameters are presented in the figure.

$$\Delta n_T = \frac{\partial n}{\partial T} \Delta T, \tag{2}$$

where $\partial n/\partial T$ is the coefficient of a temperature change in the refractive index; and ΔT is the temperature changes in the channel of the pump beam in the crystal. The amplitude of the main signal and the ratio of the fast and slow components change with changing the pump region. The main signal had the maximum amplitude when one probe beam propagated through the pumped region in the crystal. In this case the amplitude of the fast (electronic) component was much greater (approximately by an order of magnitude) than the amplitude of the slow (thermal) component. The main signal and its fast component decreased, when the pump beam was displaced from the region of the probe beam, while the thermal component was less sensitive to the displacement of the pump beam. These results well agree with the above explanation of the RIC origin. Indeed, the

electronic component is related locally with the pump beam, while the slowly relaxing thermal component – non-locally (due to thermal conductivity).

In this connection, total RICs can be represented as a sum of electronic and thermal components ($\Delta n = \Delta n_e + \Delta n_T$), the first component dominating over the second one. Changes in the populations of the electronic $^2F_{5/2}$ and $^2F_{7/2}$ levels upon pulsed pumping (pulse duration τ_p and power $P_p \approx \text{const}$) in the experiment were estimated from the expression:

$$\Delta N = \frac{\sigma_p \lambda_p P_p T_e}{hcS_p}\left[1 - \exp\left(-\frac{\tau_p}{T_e}\right)\right], \quad (3)$$

where σ_p and λ_p are the effective cross section and the pump wavelength, respectively; h is Planck's constant; c is the velocity of light; S_p is the cross sectional area of the pump region. RIC measurements, separation of components, and calculation of the excited $^2F_{5/2}$ state population from expression (3) allow us to estimate [see expression (1)] the difference of polarisabilities in the ground and excited states of ytterbium ions: $\Delta p \approx (1.9 \pm 0.8) \times 10^{-26}$ cm^3 (at the probe wavelength $\lambda_r = 633$ nm). A great scatter in the values is caused by a strong divergence of the pump beam, which leads to considerable changes in its intensity depending on the position of the Yb : YAG disk in the focal waist.

3. Measurements by the dynamic grating method

The dynamic grating in a Yb : YAG crystal was excited by 10-ns, 941-nm pulses from a Ti : Sapphire laser. The disk under study had the same dimensions and the degree of doping as that in the interferometric experiment, but its output surface had a reflection coating for pump radiation. The interference field in the crystal was formed by the replaceable diffraction beamsplitters which allowed the dynamic grating period to be stepwise changed (Fig. 4). The polarisation of pump radiation was perpendicular to the grating lines. The photo-induced dynamic grating was probed by a cw 633-nm He – Ne laser, whose polarisation coincided with the pump polarisation. Because this wavelength lies outside the absorption and gain bands of the sample, the probe radiation diffraction is caused by the phase grating induced by the pump radiation.

The time dependence $D(t)$ of the diffraction efficiency (the ratio of the power diffracted to the first radiation order to the probe radiation power) taking into account the electronic and thermal components after the pump pulse termination (in the case of $D < 1\,\%$) can be written as [9]:

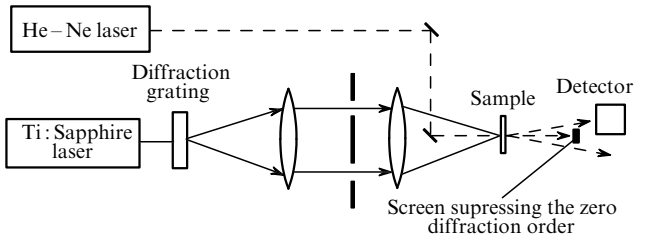

Figure 4. Scheme of the experimental setup for studying dynamic gratings.

$$D(t) = \left(\pi \int_0^l \Delta n \mathrm{d}z \Big/ \lambda_r\right)^2 = \left(\frac{\pi l}{\lambda_r}\right)^2 \left[\overline{\Delta n}_e \exp\left(-\frac{t}{T_e}\right) + \overline{\Delta n}_T \exp\left(-\frac{t}{\tau_T}\right)\right]^2, \quad (4)$$

where l is the sample thickness; $\overline{\Delta n}_e$ and $\overline{\Delta n}_T$ are the amplitudes of electronic and thermal RIC components, respectively, averaged over the sample thickness; $\tau_T = \Lambda^2/(4\pi^2\chi)$ is the time of heat transfer within the distance equal to the grating period; and χ is the thermal diffusivity.

The photoinduced RIC was experimentally studied by for three periods of the dynamic grating ($\Lambda = 53$, 39 and 26 μm) and the excitation energy density 210 – 380 mJ cm^{-2}. The typical diffraction kinetics is a sum of two components with a fast and slow decay (Fig. 5) with the amplitude of the slow component being several times greater than the amplitude of the fast component. The monotonic character of the RIC kinetics shows that the components are in-phase, i.e., RIC signs of both contributions are the same.

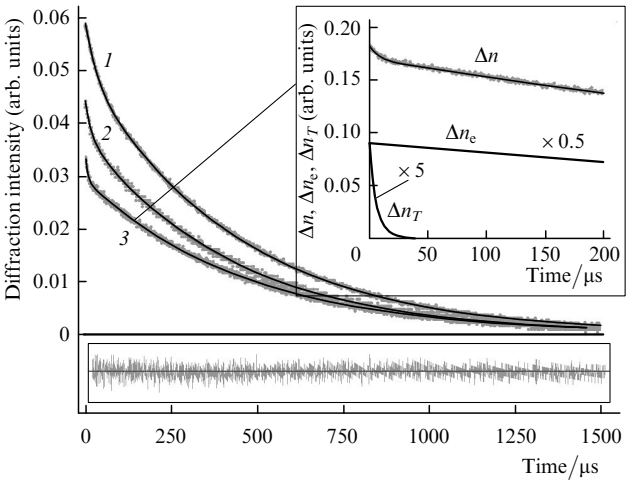

Figure 5. Experimental diffraction kinetics for $\Lambda = 52$ (*1*), 39 (*2*) and 26 μm (*3*). Solid curves are the corresponding approximations according to (*4*). The inset at the top is a time dependence Δn for curve (*3*), the inset at the bottom is the residual difference between experimental curve (*3*) and its approximation.

Approximation of the experimental data according to expression (4) yielded the relaxation time of the slow component $T_e = 900 \pm 50$ μs irrespective of the pump energy density and the grating period Λ. This value coincides with the lifetime of the upper $^2F_{5/2}$ level of Yb^{3+} ions, which allows us to identify the above component with electronic RICs appearing due to the difference in polarisabilities of Yb^{3+} ions in the ground and excited states. The relaxation time τ_T of the fast component was 29 ± 2 μs, 15 ± 3 μs and 6 ± 1 μs for $\Lambda = 53$, 39 and 26 μm, respectively. The time τ_T quadratically depends on Λ and coincides with the time of heat transfer along the range of the grating spacing (thermal diffusivity χ of the sample estimated from τ_T is 0.026 ± 0.005 cm^2 s^{-1}, which well agrees with the thermal diffusivity of a heavily-doped Yb : YAG crystal [10, 11]). Note that the electronic component had approximately the same decay time in both

measurement methods, whereas the lifetime of the thermal component in the experiment with gratings is smaller than in interferometric studies. This experimental fact can be easily explained by the difference between the grating period and the diameter of the pump beam in interferometric measurements. The measured amplitude of the total RIC increased linearly from 3.2×10^{-6} to 4.4×10^{-6} upon changing the pump energy density from 210 to 380 mJ cm^{-2}. The studies have shown that the relative thermal contribution to the total RIC [$\eta_T = \overline{\Delta n}_T/(\overline{\Delta n}_e + \overline{\Delta n}_T$] was an order of magnitude smaller than the electronic one ($\eta_T \approx 5\,\% - 8\,\%$).

Three process responsible for the heat release can be distinguished in an optically pumped Yb : YAG crystal. The first process is caused by thermalisation due to the fast (less than 10 ps) nonradiative transition from the pumped Stark level (with the energy $h\nu_p = 10624$ cm^{-1}) to the lowest Stark level (with the energy $h\nu_l = 10327$ cm^{-1}) of the upper $^2F_{5/2}$ state [3]. Because the thermalisation time is much shorter than the pulse duration, the heat release occurs during the entire pump pulse. The second process is caused by nonradiative transitions between the $^2F_{5/2}$ and $^2F_{7/2}$ levels. The heat release due to this process is determined by the population of the upper level, and its dynamics – by the lifetime of this level. The third process is related to the fast relaxation between Stark levels of the $^2F_{7/2}$ state after the relaxation of the $^2F_{5/2}$ states. The dynamics of this thermalisation process is also characterised by the lifetime of the upper level after the end of the pump pulse. Because the relaxation time of the thermal grating is, at least, 30 times smaller than the lifetime of the $^2F_{5/2}$ level, the first process dominates when the thermal grating is formed for the time $\tau_p = 10$ ns. The thermal energy of this process is a part of the absorbed energy determined by the factor $\eta_p \approx 1 - \nu_l/\nu_p$. Taking thermal and electronic process into account [from expressions (1) and (2)], expressions for Δp and the RIC temperature coefficient $\partial n/\partial T$ can be written in the form:

$$\Delta p = \eta_e \frac{9\sqrt{D(0)}n_0 hc\lambda_r}{2\pi^2(n_0+2)^2\lambda_p W_p[1-\exp(-2\alpha l)]}, \quad (5)$$

$$\frac{\partial n}{\partial T} = \eta_T \frac{\sqrt{D(0)}c_p\rho\lambda_r}{\pi W_p \eta_p[1-\exp(-2\alpha l)]}, \quad (6)$$

where η_e и η_T are relative contributions of the electronic and thermal RIC components; c_p and ρ are the specific heat and density of the Yb : YAG crystal, respectively; W_p is the energy density of the pump beam; and α is the absorption coefficient for pump radiation. By using expressions (5) and (6) and the measured diffraction efficiency $D(0)$ of the grating at the end of the pump pulse, we obtained the difference of polarisabilities $\Delta p \approx (1.95 \pm 0.25) \times 10^{-26}$ cm^3 and the thermal gradient of the refractive index $\partial n/\partial T \approx (0.7 \pm 0.2) \times 10^{-5}$ K^{-1}. A considerable scatter in the values of Δp can be explained by inaccurate measurement of the energy density in the sample due to instability of the spatial distribution of the pump beam intensity. Considerable changes in the gradient $\partial n/\partial T$ can be explained by the low amplitude of the thermal component (compared to the amplitude of the electronic component). Note also that the value Δp well agrees with the results of interferometric measurements, and the value $\partial n/\partial T$ corresponds to the results obtained in paper [10].

4. Estimate of electronic RICs near the gain resonance

We determined experimentally the polarisability difference at the probe beam wavelength $\lambda_r = 633$ nm. At the same time, the estimate of the polarisability difference at the laser transition wavelength ($\sim$1029 nm) is of considerable interest. Such a theoretical estimate of Δp(1029 nm) can be obtained with the help of the general expression for the polarisability [2]

$$p_q(\nu) = \frac{e^2}{4\pi^2 m}\sum_i \frac{f_{qi}(\nu_{qi}^2 - \nu^2)}{(\nu_{qi}^2-\nu^2)^2 + (\nu\Delta\nu_{qi})^2}$$

$$= \frac{\lambda n_0}{8\pi^2 F_L^2}\sum_i \frac{\sigma_{qi}\nu\Delta\nu_{qi}(\nu_{qi}^2-\nu^2)}{(\nu_{qi}^2-\nu^2)^2+(\nu\Delta\nu_{qi})^2}, \quad (7)$$

where e and m are the electron charge and mass, respectively; f_{qi}, σ_{qi}, ν_{qi}, and Δn_{qi} are the oscillator strength, effective cross section, frequency and linewidth of the transition between energy levels with indices q and i, respectively. The polarisability difference for $^2F_{5/2}$ and $^2F_{7/2}$ levels was calculated by considering two parts, the first one being caused by close 4f–4f transitions, and the second one – by far but strong 4f–5d transitions:

$$\Delta p(\nu) = \Delta p^{4f-4f}(\nu) + \Delta p^{4f-5d}(\nu). \quad (8)$$

The quasi-resonance component of the polarisability (related to the 4f–4f transitions) at 1029 nm was calculated from expression (7) by using the values of cross sections σ and transition linewidths $\Delta\nu$ from the literature (Table 1).

Table 1. Parameters of the electronic 4f–4f transitions in a Yb : YAG crystal used for calculating the polarisability.

Transition	λ/nm	$\Delta\nu$/cm^{-1}	$\sigma/10^{-19}$ cm^2
$^2F_{5/2} - {}^2F_{7/2}$	1048	10	0.325
	1029*, 1030***, 1031**	9	2.0375*, 2.0, 2.03**, 2.5***
	1024	7	1.15
	1007	15	0.345
	999	13	0.285
	991	7.5	0.175
	983	15	0.16
	968	8	0.525
	959	13	0.1
	941	12	0.15
	914	9	0.02
$^2F_{7/2} - {}^2F_{5/2}$	1032	7	0.11
	1028	13	0.075
	1007	13	0.045
	1001	12	0.05
	980	11	0.08
	968	8	0.71
	959	14	0.165
	941*, 940	10*, 19	0.765*, 0.8, 0.81**
	937.5	14	0.6
	929	15	0.41
	914	9	0.39

Note: *data from paper [6]; ** data from [11]; *** data from [12]; other data were obtained from Fig. 2 in paper [5].

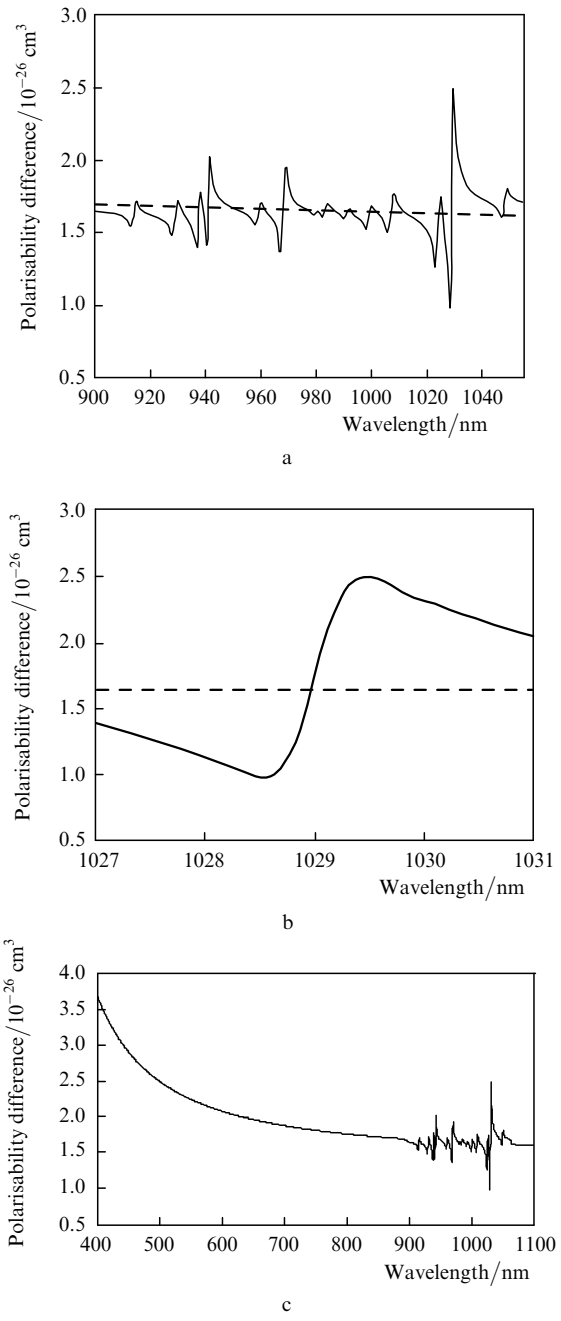

Figure 6. Numerically calculated dependences of the polarisability difference Δp on the wavelength. The dashed line in Figs 6a,b corresponds to contribution of the 4f – 5d transitions.

The calculations performed yielded $\Delta p^{4f-4f}(1029\ \text{nm}) \approx 1.1 \times 10^{-26}$ cm^3 (Fig. 6).

The nonresonance component of the polarisability (related to the 4f – 5d transitions) at 1029 nm can be calculated from the value of $\Delta p^{4f-5d}_{F7-F5}(633\ \text{nm})$ determined in the experiment. We can obtain the expression:

$$\Delta p_{F7-F5}(\nu) \approx \frac{e^2}{4\pi^2 m}\left(\frac{f_{F7-F5}}{\nu^2_{F7-5d}-\nu^2} - \frac{f_{F5-5d}}{\nu^2_{F5-5d}-\nu^2}\right) \qquad (9)$$

for estimates from general expression (7) at the probe frequency ν, which is far away from the 4f – 5d resonances, where f_{F7-5d} and f_{F5-5d} are the oscillator strengths; ν_{F7-5d} and ν_{F5-5d} are transition frequencies from the $^2F_{7/2}$ and $^2F_{5/2}$ levels to the 5d-shell levels, respectively.

By using expression (9) (under the assumption that the oscillator strengths of the 4f – 5d transitions are equal: $f_{F7-5d} \approx f_{F5-5d}$), knowing the transition frequency $\nu^{4f-5d} \approx 210$ nm [13], and the value of $\Delta p^{4f-5d}_{F7-F5}(633\ \text{nm}) \approx 2.0 \times 10^{-26}$ cm^3, we can obtain the numerical estimate: $\Delta p^{4f-5d}_{F7-F5}(1029\ \text{nm}) \approx 1.63 \times 10^{-26}$ cm^3. Comparison of $\Delta p^{4f-4f}(1029\ \text{nm})$ and $\Delta p^{4f-5d}_{F7-F5}(1029\ \text{nm})$ shows that the second component considerably dominates. This is also valid for other transition frequencies near the gain line in the Yb : YAG crystal (Fig. 6).

The ratio of the real and imaginary parts of the cubic susceptibility $\chi^{(3)}$ at 1029 nm determined by the expression $\beta = \text{Re}\,\chi^{(3)}/\text{Im}\,\chi^{(3)} = 8\pi^2 F_L^2 \Delta p/(n_0 \lambda \sigma_e)$ (where $\sigma_e = 2.1 \times 10^{-20}$ cm^2 is the cross section of the laser transition) can be estimated as $\beta \approx 1.0$ [$\Delta p(1029\ \text{nm}) \approx 1.63 \times 10^{-26}$ cm^3], which is almost an order of magnitude greater than for the Nd : YAG crystal [2 – 4]. This should lead to stronger manifestations of the lens caused by changes in the population and the grating of electronic RICs in the Yb : YAG crystal compared to Nd : YAG crystal.

5. Conclusions

Our experiments have shown that the strong RIC in intensely pumped Yb : YAG crystals consists of the electronic and thermal components. Electronic RICs caused by a change in the polarisability of Yb^{3+} ions in the Yb : YAG disk pumped by laser pulses were an order of magnitude greater than thermal changes. The dominant contribution to the polarisability difference for excited and nonexcited Yb^{3+} ions both at the probe wavelength of 633 nm and at the gain transition wavelength of 1029 nm is provided by the wings of strong transitions between the electronic 4f and 5d shells (whose resonances lie in the UV region) (Fig. 6c). The polarisability difference for Yb^{3+} ions at the working transition levels ($^2F_{7/2}$ and $^2F_{5/2}$) is 2.5 times smaller than that for Nd^{3+} ions (at the $^4I_{9/2}$ and $^4F_{3/2}$ levels). However, when the atomic concentration of doping Yb^{3+} ions is 9 %, electronic RICs in the Yb : YAG crystal noticeably exceed similar changes in the Nd : YAG crystal (with the atomic concentration of doping Nd^{3+} ions equal to ~1 %).

Electronic RICs, which are a local factor independent of the size of the active Yb : YAG-crystal element and the pump geometry, can considerably exceed thermal RICs in the case of a narrow pump beam or in thin disks with a restricted heating. The electronic components are identical in a crystal upon pulsed or cw pumping, although the thermal contribution can increase proportionally to the thermal relaxation time. The temporal behaviour and spatial peculiarities of the electronic and thermal RICs differ from each other, therefore, lenses caused by changes in the population levels in intensely pumped active elements should be calculated separately. Relatively 'strong' refractive-index gratings (which are determined by the dominant electronic component) cannot be neglected compared to the gain gratings in nonlinear optical interactions in Yb : YAG lasers and, in particular, in lasers with a resonator formed by dynamic gratings [14].

Acknowledgements. This work was supported by INTAS (Grant No. 03-51-4893), the program 'Nonlinear Optics of

Unique Laser Systems' of the Department of Physical Sciences of RAS and the State Program of Applied Studies of Belarus (Grant No. P1.16).

References

1. Powel R.C. *Physics of Solid-State Laser Materials* (New York – Berlin – Heidelberg: Springer-Verlag, 1998).
2. Antipov O.L., Kuzhelev A.S., Luk'yanov A.Yu., Zinov'ev A.P. *Kvantovaya Elektron.*, **25** (10), 891 (1998) [*Quantum Electron.*, **28** (10), 867 (1998)].
3. Antipov O.L., Eremeykin O.N., Savikin A.P. *Kvantovaya Elektron.*, **33** (10), 861 (2003) [*Quantum Electron.*, **33** (10), 861 (2003)].
4. Antipov O.L., Eremeykin O.N., Savikin A.P., Vorob'ev V.A., Bredikhin D.V., Kuznetsov M.S. *IEEE J. Quantum Electron.*, **39**, 910 (2003).
5. Krupke W.F. *IEEE J. Sel. Top. Quantum Electron.*, **6**, 1287 (2000).
6. Bruesselbach H.W., Sumida D.S., Reeder R.A., Byren R.W. *IEEE J. Sel. Top. Quantum Electron.*, **3**, 105 (1997).
7. Stewen C., Contag K., Larionov M., Giesen A., Hügel H. *IEEE J. Sel. Top. Quantum Electron.*, **6**, 650 (2000).
8. Bochove E. *Opt. Lett.*, **29**, 2414 (2004).
9. Eichler H.J., Gunter P., Pohl D.W. *Laser-Induced Dynamic Gratings* (New York – Berlin – Heidelberg: Springer-Verlag, 1986).
10. Dong J., Deng P., Liu Y., Zhang Y., Xu J., Chen W., Xie X. *Appl. Opt.*, **40**, 4303 (2001).
11. DeLoach L.D., Payne S.A., Chase L.L., Smith L.K., Kway W.L., Krupke W.F. *IEEE J. Quantum Electron.*, **29**, 1179 (1993).
12. Spühler G.J., Pachotta R., Kullberg M.P., Moser M., Mix E., Huber G., Harder C., Keller U. *Appl. Phys. B*, **72**, 285 (2001).
13. Pieterson L., Heeroma M., Heer E., Meijerink A. *J. Luminesc.*, **91**, 177 (2001).
14. Antipov O.L., Eremeykin O.N., Ievlev A.V., Savikin A.P. *Opt. Express*, **12** (18), 4313 (2004).